Novel Preconditioners for Unfitted FEM in DarcyFlow for Fractured Medium

Wasif Khan

 Government College University, Lahore

Shahbaz Ahmad

 shahbazahmad@sms.edu.pk

 Government College University, Lahore

Additional Declarations: No competing interests reported.

Novel Preconditioners for Unfitted FEM in Darcy Flow for Fractured Medium

Wasif Khan*and Shahbaz Ahmad†

Abstract

We suggest using GMRES preconditioners to solve a saddle-point problem arising from the discretization of unfitted Finite Element Method (FEM) in Darcy flow for fractured media. These problems often occur when we use a specific method to understand how fluids move in complex situations, such as multiple dimensions. We conducted a thorough study, examining the solutions, and found that our new way of preparing the problem makes things work better. Spectral analysis of the proposed preconditioners, along with numerical results, showed that our method works well, especially when combined with a flexible-GMRES method. We applied our approach to solve problems from a 2D test scenario, proving that our way is practical and useful.

keywords: Darcy flow problem, Finite Element Method, Spectral analysis, Preconditioning Technique, Krylov Subspace Methods.

AMS Classification: 74Sxx, 65N06, 65N12, 65F10.

1 Introduction

The computational simulation of fluid flow within porous media containing fractures presents a widespread challenge in geosciences and reservoir behavior modeling [25, 43]. Despite a rich body of literature on this subject, as highlighted in recent research summaries such as [3, 15, 21, 26, 35], the development of a precise and efficient numerical approach for handling intricate fracture networks remains a formidable obstacle.

---

*ASSMS, Government College University, Lahore, Pakistan (`wasif_khan_22@sms.edu.pk`)

†ASSMS, Government College University, Lahore, Pakistan (`shahbazahmad@sms.edu.pk`)

Recent publications have explored finite element techniques that do not specifically cater to the geometric characteristics when modeling fluid and substance movement in permeable media with fractures, as evidenced in works like [6, 14, 27, 34]. Notable developments aligned with the approach discussed in this paper are apparent in [23, 28, 33]. In [28], a low-order Raviart–Thomas finite element method was employed for addressing Darcy flow in a 1D network of fractures. Although triangulations were constructed for each fracture surface, they did not align with the intersection points of fractures. To manage solution discontinuities at junctions, the XFEM methodology was employed. A comprehensive review of this and other numerical approaches, assuming varying degrees of conformity in fracture mesh interfaces, is available in [30]. Triangulating each fracture branch proves challenging, especially in the case of extensive networks or intricate geometries. Consequently, the next level of nonconformity involves departing from the conventional triangulation of fractures. Instead, the flow problem is discretized exclusively along the fracture network, utilizing degrees of freedom tailored to the ambient mesh, ensuring complete separation of the background mesh from the embedded fracture network. This innovative strategy was initially introduced in [39] and has evolved into the Trace Finite Element Method (FEM) for addressing scalar elliptic partial differential equations (PDEs) on surfaces [38], forming a component of the Cut FEM [16]. The Trace FEM methodology has found application in modeling the transport and diffusion of contaminants in fractured porous media, as demonstrated in [23]. In addressing the Darcy problem, the Trace Finite Element Method (FEM) was first explored in [33], where the authors focused on solving the Darcy problem on a surface embedded within a volumetric tetrahedral grid, utilizing a modified form of the Hughes–Masud weak formulation to compute pressure and tangential velocity.

Building upon the groundwork laid in [33], we apply the Trace Finite Element Method (FEM) alongside a modified version of the Hughes–Masud weak formulation. Our current study stands out in two crucial aspects. Firstly, we embrace octree Cartesian grids for the ambient mesh, ensuring convenient adaptability. Secondly, and notably, we delve into the realm of intersecting piecewise smooth surfaces representing branching fractures, in contrast to previous work that focused solely on closed smooth manifolds. Introducing branching surfaces leads to discontinuous fluxes and a piecewise smooth pressure field. Addressing these challenges without relying on mesh fitting while maintaining optimal convergence order is a non-trivial task. In our manuscript, we tackle this issue by allowing discontinuities in both velocity and pressure fields within the background cells intersected by fracture junctions, achieved through the incorporation of a penalty term. Our strategy for managing fracture junctions shares similarities with the Nitsche-XFEM method introduced by Hansbo and Hansbo [32] for handling interface problems and aligns

2

with the broader concept of CutFEM [16]. Notably, our distinctive approach involves using a different scaling technique for the penalty term. Additionally, we diverge by omitting specific consistency terms, common in discontinuous Galerkin FEM and Nitsche's method, along the junctions. Remarkably, despite these variations, we consistently maintain optimal asymptotic accuracy in our methodology.

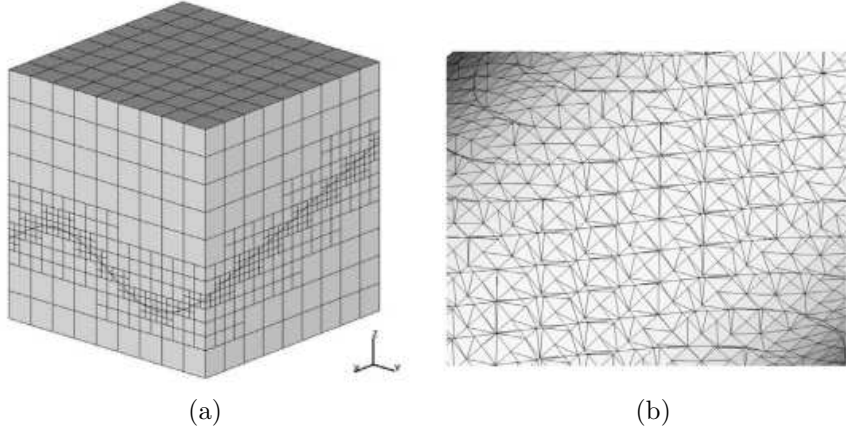(a)   (b)

Figure 1: (a) An instance of a bulk domain featuring a singular fracture, wherein the background mesh undergoes refinement in close proximity to the fracture. (b) The magnified view of the surface triangulation generated for numerical integration. [22]

Incorporating interaction conditions introduces interdependence and asymmetry into the Darcy model, primarily due to its saddle-point formulation. Consequently, employing the Trace finite element method in conjunction with this model generates a set of algebraic equations characterized by interdependence, indefiniteness, asymmetry, and ill-conditioning. To tackle this computational hurdle, we employ the generalized minimal residual (GMRES) method with preconditioning, as suggested by [18, 19], as a viable solution strategy for the discretized system.

Significant research efforts have been dedicated to advancing preconditioning techniques tailored specifically for saddle-point problems. Various existing preconditioners in the literature are formulated and assessed with a comprehensive algebraic perspective, applicable to generic saddle-point problems. While certain preconditioners rely on a singular model, such as a Stokes operator, to address fluid flow, a limited number address the integration of diverse models and their interconnected interfaces.

Our focus centers on devising effective and highly operational decoupled preconditioning techniques that fully exploit the inherent mathematical structures of

3

distinct mixed physical models. This entails meticulous consideration of the analytical properties of local Darcy operators and their interactions at interfaces. Our goal is to introduce multiple preconditioners specifically designed for the Darcy model, where preconditioning not only acts as a decoupling mechanism but also contributes to enhancing the convergence rate [10, 17, 20]. The manuscript will offer a theoretical analysis and present numerical experiments to highlight the effectiveness and efficiency of the proposed decoupled preconditioners. Additionally, we will explore how variations in physical parameters impact the convergence performance.

2   Mathematical model

Consider a fragmented and smooth surface denoted as $\hat{\Gamma}$ within a specified bulk domain $\hat{\Omega} \subset \mathbb{R}^3$. This surface $\hat{\Gamma}$ represents a 2D fracture network, comprising numerous interconnected components expressed as $\hat{\Gamma} = \bigcup_{j=1}^{n} \hat{\Gamma}_j$. Each $\hat{\Gamma}_j$ is conceptualized as a smooth, orientable surface without self-intersections. For analytical purposes, we assume that every $\hat{\Gamma}_j$ is a subdomain of a more extensive C^2–smooth surface $\hat{\Gamma}_j$ with $\partial \hat{\Gamma}_j \cap \hat{\Omega} = \emptyset$. Additionally, $\partial \hat{\Gamma}_j$ is a piece-wise smooth and Lipschitz curve within $\hat{\Gamma}_j$. The individual components $\hat{\Gamma}_j$ only intersect by a curve, i.e., $\text{meas}^2(\hat{\Gamma}_j \cap \hat{\Gamma}_i) = 0$ for $j \neq i$, and $\hat{\Gamma}_j \cap \hat{\Gamma}_i = \emptyset$ for $j \neq i$. This condition implies that fracture parts separated by a junction are considered distinct components. Moreover, let m represent a unit normal vector defined across the entire surface $\hat{\Gamma}$ except at junction interfaces. Specifically, we represent m_j as m on $\hat{\Gamma}_j$, extending similar notation to other vector and scalar fields defined on the union of surfaces $\bigcup_{j=1}^{n} \hat{\Gamma}_j$.

The representation of fractures as 2D interfaces in porous media flow has been extensively studied in the literature, as demonstrated by various works [1, 2, 29, 36]. In this context, the movement within the fracture component $\hat{\Gamma}_j$ is defined by the tangential velocity field $u_j(x)$, representing the flow rate through the cross-section of the fracture, and the pressure field $p_j(x)$ for $x \in \hat{\Gamma}_j$. The Darcy systems govern the steady-state flow within $\hat{\Gamma}$.

$$
\begin{cases}
K_j^{-1} u_j + \nabla_{\hat{\Gamma}} p_j = f_j \\
\text{div}_{\hat{\Gamma}} u_j = g & \text{in } \hat{\Gamma}_j, \quad (j = 1, \ldots, n) \\
u_j \cdot n_j = 0
\end{cases}
\tag{1}
$$

In conjunction with the provided conditions at the interface and boundaries of the computational domain, the equation (1) and subsequent discussions in the manuscript utilize $\nabla_{\hat{\Gamma}}$ and $\text{div}_{\hat{\Gamma}}$ to represent the operators for surface tangential gradient and divergence, respectively. Within this context, the term g signifies

the source term, typically originating from fluid exchange with the porous matrix (though not addressed in this paper). The external force per unit area, represented by f_j, acts tangentially to $\hat{\Gamma}_j$, and its direction aligns with the tangential plane. The symmetric permeability tensor along the fracture is denoted as K_j. For any tangential vector field v (i.e., $v \cdot n_j = 0$), where n_j is the normal vector, it satisfies the condition $v^T K_j v \geq \zeta_j |v|^2$ with some $\zeta_j > 0$, and $n_j^T K_j v = 0$. Consequently, $K_j^{-1} v$ exists for a tangential field v. It is noteworthy that the incorporation of fracture aperture into K_j can be achieved through scaling, as discussed in [1].

In the scenario where $\hat{\Gamma}$ is piece-wise smooth, there are additional considerations, especially when dealing with fracture networks where the edges, or fracture junctions, play a crucial role. Let's focus on an edge denoted as $\hat{e}$, which is shared by $M_{\hat{e}}$ smooth components $\hat{\Gamma}_{jl}$, each associated with an index $(l = 1, \ldots, M_{\hat{e}})$. The set $(\{jl\}_{l=1,\ldots,M_{\hat{e}}})$ represents a subset of indices from $(1, \ldots, n)$ unique to each $\hat{e}$. The normal vector on the boundary $\partial \hat{\Gamma}_j$ is oriented within the tangential plane of $\hat{\Gamma}_j$ and points outward. The conservation of fluid mass can be articulated as:

$$\sum_{l=1}^{M_{\hat{e}}} u_{jl} \cdot m_{jl} = 0 \text{ on } \hat{e}, \tag{2}$$

This requirement, as stated in the second condition at the interface, ensures pressure continuity along $\hat{e}$:

$$p_{j_1} = \ldots = p_{j_{M_{\hat{e}}}} \text{ on } \hat{e}. \tag{3}$$

Consider the set $\hat{E}$, which includes the intersection points of fractures. It is reasonable to assume that $\hat{E}$ is a finite set, and for any $\hat{e} \in \hat{E}$, the measure of $\hat{e}$, denoted as $\text{meas}_1(\hat{e})$, satisfies $0 < \text{meas}_1(\hat{e}) < +\infty$.

Finally, we specify pressure constraints at the boundary on $\partial \hat{\Gamma}_d$ and enforce the boundary condition for flux $\partial \hat{\Gamma}_n$, where $\partial \hat{\Gamma} = \partial \hat{\Gamma}_d \cup \partial \hat{\Gamma}_n$:

$$\begin{cases} n_j \cdot u_j = \phi_j \text{ on } \partial \hat{\Gamma}_n \cap \partial \hat{\Gamma}_j, \quad (j = 1, \ldots, n) \\ p = p_d \text{ on } \partial \hat{\Gamma}_d. \end{cases} \tag{4}$$

3   Finite element method

Initially, let's assume the existence of a discretization denoted as $\mathcal{T}_{\delta h}$ for the volumetric domain $\hat{\Omega}$ (matrix). This discretization involves a consistent subdivision into tetrahedra with shape-regular properties. Our focus is on a Cartesian background mesh characterized by cubic cells, showcasing flexibility through local refinement

achieved by iteratively subdividing each cubic cell into eight smaller cubic subcells. This iterative process results in a grid structure following an octree hierarchy, providing a versatile foundation for our study. This mesh serves as the discretization $\mathcal{T}_{\delta h}$ for the volumetric domain $\hat{\Omega}$, where $\hat{\Omega} = \bigcup_{T \in \mathcal{T}_{\delta h}} T$. The fracture network $\hat{\Gamma} \subset \hat{\Omega}$ is allowed to intersect this mesh arbitrarily. For analytical considerations, we assume that the cells intersected by $\hat{\Gamma}$ have a quasi-uniform size characterized by the characteristic size δh.

Now, consider the ambient finite element space, encompassing all piecewise trilinear continuous functions defined on the bulk octree mesh $\mathcal{T}_{\delta h}$.

$$V_{\delta h} := \{\hat{v} \in C(\hat{\Omega}) \,|\, \hat{v}|_S \in P_1 \,\forall\, S \in \mathcal{T}_{\delta h}\}, \tag{5}$$

where $P_1 = \text{span}\{1, \psi_1, \psi_2, \psi_3, \psi_1\psi_2, \psi_1\psi_3, \psi_2\psi_3, \psi_1\psi_2\psi_3\}$.

For every fracture $\hat{\Gamma}_j$ in the network $\hat{\Gamma}$, we define the subregion of $\hat{\Omega}$ formed by all cells intersected by $\hat{\Gamma}_j$.

$$\hat{\Omega}_{j\delta h} = \bigcup T \in \mathcal{T}_{\delta h} : T \cap \hat{\Gamma}_j \neq \emptyset,$$

Additionally, elucidate the constraints and outline any restrictions associated with the proposed methodology of $V_{\delta h}$ to $\hat{\Omega}_{j\delta h}$, representing the set of functions that are continuous and defined on distinct trilinear pieces, forming a piecewise structure.

$$V_{\delta h}^j := \{\hat{u} \in C(\hat{\Omega}_{\delta h}^j) \,|\, \exists \hat{v} \in V_{\delta h} \text{such that} \hat{u} = \hat{v}|_{\hat{\Omega}_{\delta h}^j}\}. \tag{6}$$

Our spaces for trial and testing finite elements are constructed using $V_{\delta h}^j$. We specify the pressure and velocity function spaces as follows:

$$V_{\delta h} = \prod_{j=1}^n [V_{\delta h}^j] \quad \text{and} \quad U_{\delta h} = \prod_{j=1}^n [V_{\delta h}^j]^3.$$

According to the Trace FEM approach, the solutions to the equations (1)-(4) utilizing finite elements will manifest as traces of functions derived from $P_{\delta h}$ and $U_{\delta h}$ on $\hat{\Gamma}$. However, the finite element formulation will express these functions in relation to $\bigcup_{j=1}^n \hat{\Omega}_{\delta h}^j$. Consequently, this approach gives rise to a system of algebraic equations concerning standard nodal degrees of freedom within the overarching mesh $\mathcal{T}_{\delta h}$.

Furthermore, we use the symbol $((\cdot, \cdot)_P)$ to denote the (L^2) scalar product across a region (P), which might signify a 3D, 2D, or 1D manifold depending on the context. For example, utilizing this expression, the Green formula on $\hat{\Gamma}_j$ can be formulated as:

$$(\text{div}_{\hat{\Gamma}} \hat{v}, p)_{\hat{\Gamma}_j} = -(\hat{v}, \nabla_{\hat{\Gamma}} p)_{\hat{\Gamma}_j} + (n_j \cdot \hat{v}, p)_{\partial \hat{\Gamma}_j} \tag{7}$$

For any smooth vector field tangent to the surface $\hat{v}$ and scalar field (p) on (Γ_j), the expression holds true.

The suggested finite element approach broadens the stabilized mixed formulation for the Darcy problem, initially introduced in [37], originally designed for planar domains. The pivotal observation lies in the fact that the smooth solution to equations (1)-(4) satisfies the identity.

$$(K_j^{-1}u + \nabla_{\hat{\Gamma}}q, \hat{v})_{\hat{\Gamma}_i} + (\text{div}_{\hat{\Gamma}}u, p)_{\hat{\Gamma}_i} + \frac{1}{2}(K_j^{-1}u + \nabla_{\hat{\Gamma}}q, -\hat{v} + K_j\nabla_{\hat{\Gamma}}p)_{\hat{\Gamma}_j}$$
$$= (g, p)_{\hat{\Gamma}_j} + \frac{1}{2}(f, -\hat{v} + K_j\nabla_{\hat{\Gamma}}p)_{\hat{\Gamma}_j}$$

For all $p \in H^1(\hat{\Gamma}_j)$, $\hat{v} \in L^2(\hat{\Gamma}_j)$, and $(j = 1, \ldots, n)$, the expression (7) is applied. Setting $(p = 0)$ on $\partial\hat{\Gamma}_d$ and conducting straightforward calculations, this yields:

$$(K_j^{-1}u, \hat{v})_{\hat{\Gamma}_j} + (\nabla_{\hat{\Gamma}}q, \hat{v})_{\hat{\Gamma}_j} - (\nabla_{\hat{\Gamma}}p, u)_{\hat{\Gamma}_j} + (K_j\nabla_{\hat{\Gamma}}q, \nabla_{\hat{\Gamma}}p)_{\hat{\Gamma}_j}$$
$$+ 2(n_j \cdot u, p)_{\partial\hat{\Gamma}_j} = 2(g, p)_{\hat{\Gamma}_j} + (f, -\hat{v} + K_j\nabla p)_{\hat{\Gamma}_j} \tag{8}$$

Another valuable insight is that (q) and (p) can be recognized by their normal extensions to a vicinity of $\hat{\Gamma}_j$ for every (j). This recognition, assumed throughout the paper, implies the equality $\nabla_{\hat{\Gamma}}q = \nabla q$. This equality can be further employed in (8) to derive:

$$(K_j^{-1}u, \hat{v})_{\hat{\Gamma}_j} + (\nabla q, \hat{v})_{\hat{\Gamma}_j} - (\nabla p, u)_{\hat{\Gamma}_j} + (K_j\nabla q, \nabla p)_{\hat{\Gamma}_j}$$
$$+ 2(m_j \cdot u, p)_{\partial\hat{\Gamma}_j} = 2(g, p)_{\hat{\Gamma}_j} + (f, -\hat{v} + K_j\nabla p)_{\hat{\Gamma}_j} \tag{9}$$

This corresponds to the comprehensive gradient representation of the surface partial differential equations (PDEs), as elucidated in [24, 40]. The full gradient formulation leverages the inclusion of $\hat{\Gamma}$ within the surrounding Euclidean space, enhancing stability in a broader context. This formulation is particularly well-suited for finite element methods built upon external elements. It maintains consistency across various ambient finite element methods aimed at approximating both the surface solution and its normal extension. In the context of the surface Darcy problem, the full gradient formulation demonstrated its efficacy in [33]. To summarize, through the aggregation of equalities (9) for all $(j = 1, \ldots, n)$ and the incorporation of the interface condition (2), along with the flux boundary condition derived from

(4), we infer that any smooth solution of (1)—(4) adheres to:

$$(K^{-1}u, \hat{v})_{\hat{\Gamma}} + (\nabla q, \hat{v})_{\hat{\Gamma}} - (\nabla p, u)_{\hat{\Gamma}} + (K_j \nabla q, \nabla p)_{\hat{\Gamma}}$$

$$+ \sum_{\hat{e} \in \hat{E}} \frac{2}{M_{\hat{e}}} \sum_{l=1}^{M_{\hat{e}}-1} \sum_{k=l+1}^{M_{\hat{e}}} (m_{jl} \cdot u_{jl} - n_{jk} \cdot u_{jk}, p_{jl} - p_{jk})_{\hat{v}} \tag{10}$$

$$= 2(g, p)_{\hat{\Gamma}} + (f, -\hat{v} + K_j \nabla p)_{\hat{\Gamma}} - 2(\Phi, p)_{\partial \hat{\Gamma}_n}$$

For any $p \in \prod_{j=1}^{n} H^1(\hat{\Gamma}_j)$ with $p = 0$ on $\partial \hat{\Gamma}_d$, and $\left(\hat{v} \in L^2(\hat{\Gamma})^3 \right)$, addressing the summation of the contributions from the edges involves the utilization of (2) alongside the following identity:

$$\sum_{j=1}^{M} a_j b_j = \left(\frac{1}{M} \right) \left[\left(\sum_{j=1}^{M} a_j \right) \left(\sum_{j=1}^{M} b_j \right) + \left[\sum_{j=1}^{M-1} \sum_{i=j+1}^{M} (a_j - a_i)(b_j - b_i) \right] \right] \quad (\forall a_i, b_i \in \mathbb{R}) \tag{11}$$

Our finite element approach relies on the equality (10). It's noteworthy that we presume the extension of (K_j) to possess positive definiteness and symmetry when extended to $(\mathbb{R}^3)$, rather than exclusively in the tangential space. This extension doesn't impact any quantities in (10) but proves beneficial in subsequent stages of the finite element formulation. To approximate pressure, we employ finite element functions from $(P_{\delta h})$, featuring discontinuities across $\hat{e} \in \hat{E}$. Consequently, we introduce a penalty term to our formulation to weakly enforce the pressure continuity condition from (4). Furthermore, we choose over-penalization by opting for a distinct scaling of the penalty parameter, in contrast to the conventional approach in Nitsche's [32] or methods based on the discontinuous Galerkin approach [4]. Intriguingly, this over-penalization allows us to bypass other edge terms in the finite formulation, significantly simplifying the method while preserving optimal consistency order.

The aforementioned equation (10) can be decomposed into two linear equations as follows:

$$(K^{-1}u, \hat{v})_{\hat{\Gamma}} + (\nabla q, \hat{v})_{\hat{\Gamma}} = (f, -\hat{v} + K_j \nabla p)_{\hat{\Gamma}} - 2(\Phi, p)_{\partial \hat{\Gamma}_n}, \tag{12}$$

$$-(\nabla p, u)_{\hat{\Gamma}} + (K_i \nabla q, \nabla p)_{\hat{\Gamma}} + \sum_{\hat{e} \in \hat{E}} \rho_{\hat{e}} \delta h^2 \sum_{l=1}^{M_e-1} \sum_{j=k}^{M_{\hat{e}}} (q_{jl} - q_{jk}, p_{jl} - p_{jk})_{\hat{e}} +$$

$$\sum_{j=1}^{n} \rho u_{\delta h}(m_j \cdot \nabla u_j, m_j \cdot \nabla \hat{v}_j)_{\hat{\Omega}_{\delta h}^j} + \sum_{j=1}^{n} \rho q_{\delta h}(m_j \cdot \nabla q_j, m_j \cdot \nabla p_j)_{\hat{\Omega}_{\delta h}^j} = 2(g, p)_{\hat{\Gamma}} \tag{13}$$

The parameters ρ are tunable, and for both the investigation and experiments, we set them to a constant value of 1. The term $I_b^{\delta h}(q_d)$ denotes the representation of the boundary condition through interpolation. This process of interpolation extends pressure values from $\partial \hat{\Gamma}_d$ in the normal directions within $\partial \hat{\Omega}$ to the relevant nodal values originating from the intersection of $\hat{\Omega}_j^{\delta h}$ and $\partial \hat{\Omega}$.

Consequently, the linear system of equations in (12)–(13) can be represented in matrix form as:

$$\begin{bmatrix} M & C \\ C^T & W \end{bmatrix} \begin{bmatrix} U \\ P \end{bmatrix} = \begin{bmatrix} f \\ g \end{bmatrix} \tag{14}$$

Where, $(M_{ij} = (K^{-1}\psi_j, \psi_l), l = 1,2,3,\cdots,n)$, $(C_{ij} = (\nabla\phi_k, \psi_j), k = 1,2,3,\cdots,m$ and $j = 1,2,3,\cdots,n)$. $W_{ik} = (K\nabla\phi_k, \nabla\phi_l) + t_{lk}$, Where t_{ik} are the elements from the discretization of the summation terms in (13). Also, $[\hat{u_1}, \hat{u_2}, \cdots, \hat{u_n}]^T$, and $P = [p_1, p_2, \cdots, p_n]^T$.

4 Proposed Preconditioned Matrix

This section begins by presenting fundamental concepts and core principles related to iterative techniques. Suppose $A \in \mathbb{R}^{N \times N}$ has an arbitrary decomposition ($A = P - R$), where P is non-singular [5, 7–9]. In the context of this decomposition, a foundational iterative approach to address the system equation (14) manifests itself in the subsequent manner:

$$x^{(k+1)} = P^{-1}b + P^{-1}Rx^{(k)} \qquad (k = 0, 1, 2, ...), \tag{15}$$

The iterative process (15) demonstrates convergence when initiated with any starting point $x^{(0)} \in \mathbb{R}^n$, solely contingent on the condition that the spectral radius of the iteration matrix $P^{-1}R$ remains strictly below one.

Now we investigate a partitioning strategy for the coefficient matrix in (14),

$$A = \begin{bmatrix} M & C \\ C^T & W \end{bmatrix}. \tag{16}$$

Consider

$$A = P_1 - R \tag{17}$$

where,

$$P_1 = \begin{bmatrix} M & 0 \\ -C^T & W - C^T M^{-1} C \end{bmatrix}, \quad R = \begin{bmatrix} 0 & -C \\ 0 & -C^T M^{-1} C \end{bmatrix} \tag{18}$$

9

To address the system (14), we can devise the subsequent iterative scheme.

$$x^{(k+1)} = P_1^{-1} b + G x^{(k)}, \qquad (k = 0, 1, 2, ...,) \qquad (19)$$

$x^0 \in \mathbb{R}^{m+n}$ represents an arbitrary initial estimate, and the matrix G is

$$G = P_1^{-1} R = \begin{bmatrix} M & 0 \\ -C^T & W - C^T M^{-1} C \end{bmatrix}^{-1} \begin{bmatrix} 0 & -C \\ 0 & -C^T M^{-1} C \end{bmatrix} \qquad (20)$$

The matrix P_1 in (18) can be decomposed into the form:

$$P_1 = \begin{bmatrix} I & 0 \\ -C^T M^{-1} & I \end{bmatrix} \begin{bmatrix} M & 0 \\ 0 & W - C^T M^{-1} C \end{bmatrix} \qquad (21)$$

From the above decomposition, It is readily apparent that the matrix P_1 is invertible and we have,

$$P_1^{-1} = \begin{bmatrix} M & 0 \\ 0 & W - C^T M^{-1} C \end{bmatrix}^{-1} \begin{bmatrix} I & 0 \\ C^T M^{-1} & I \end{bmatrix} \qquad (22)$$

Theorem 1 *Assume that M is a positive definite symmetric matrix with dimensions $m \times m$, Let C be a full-rank Toeplitz matrix with dimensions $m \times n$. In this scenario, regardless of the initial estimate, the iterative method (19) converges to the unique solution.*

Proof:
Considering the relation expressed in (22), we obtain

$$G = P_1^{-1} R = \begin{bmatrix} M & 0 \\ 0 & W - C^T M^{-1} C \end{bmatrix}^{-1} \begin{bmatrix} I & 0 \\ C^T M^{-1} & I \end{bmatrix} \begin{bmatrix} 0 & C \\ 0 & -C^T M^{-1} C \end{bmatrix}$$

$$= \begin{bmatrix} M^{-1} & 0 \\ 0 & (W - C^T M^{-1} C)^{-1} \end{bmatrix} \begin{bmatrix} 0 & C \\ 0 & 0 \end{bmatrix}$$

$$= \begin{bmatrix} 0 & -M^{-1} C \\ 0 & 0 \end{bmatrix}$$

We deduce that all the eigenvalues associated with the matrix G equate to zero. As a result, we establish spectral radius $\rho(G) < 1$, confirming the theorem's validity.

Typically, the effectiveness of the iterative scheme (19) in converging may not be optimal for solving the system (14). Our primary focus involves leveraging the

matrix P_1 as a preconditioner to enhance the efficiency of Krylov subspace methods, such as GMRES.

The incorporation of the preconditioner P_1 necessitates addressing a linear subsystem in the subsequent stages.

$$P_1 z = r = \begin{bmatrix} M & 0 \\ 0 & W - C^T M^{-1} C \end{bmatrix} \begin{bmatrix} I & 0 \\ C^T M^{-1} & I \end{bmatrix} \begin{bmatrix} z_1 \\ z_2 \end{bmatrix} \tag{23}$$

$$P_1 z = r = \begin{bmatrix} r_1 \\ r_2 \end{bmatrix}$$

Subsequently, we can outline a straightforward algorithm for computing $z = P_1^{-1} r$ as follows.

Algorithm 1: Calculation of $z = P_1^{-1} r$

---

1. Solve, $M z_1 = r_1 \quad$ for $\quad z_1$;

2. Set, $(W - C^T M^{-1} C) z_2 = C^T M^{-1} r_1 + r_2$.

Theorem 2 *Consider a symmetric positive definite matrix M and a full-rank Toeplitz matrix C, with dimensions $(m \times m)$ and $(m \times n)$ respectively. Then the preconditioner P_1 satisfies*

$$\sigma(P_1^{-1} A) = 1,$$

where $\sigma(.)$ denotes the set of all eigenvalues of a matrix.

Proof:

It is straightforward to confirm that

$$P_1^{-1} A = I - P_1^{-1} R = \begin{bmatrix} I & -M^{-1} C \\ 0 & I \end{bmatrix}. \tag{24}$$

This complete theorem.

Certainly! To enhance our result, let's extend our results in a manner that ensures all blocks are non-zero. This generalization will provide a more comprehensive and inclusive perspective, ensuring that each block contributes meaningfully to the overall outcome. Indeed, our generalized preconditioner matrix is denoted as P_2, from the partitioning

$$A = P_2 - R \tag{25}$$

11

where

$$P_2 = \begin{bmatrix} M & 2C \\ -C^T & W - C^T M^{-1} C \end{bmatrix}, \quad R = \begin{bmatrix} 0 & C \\ 0 & -C^T M^{-1} C \end{bmatrix} \tag{26}$$

This preconditioner P_2 has been crafted to accommodate a scenario where all blocks are non-zero, thus facilitating a more robust and versatile solution. The application of this preconditioner matrix aims to enhance the efficiency and reliability of our computations, ensuring that every block plays a significant role in optimizing the overall performance.

To address the system (14), so we can devise the subsequent iterative scheme.

$$x^{(k+1)} = P_2^{-1} b + G x^{(k)}, \qquad (k = 0, 1, 2, ...,) \tag{27}$$

$x^0 \in \mathbb{R}^{m+n}$ represents an arbitrary initial estimate, and the matrix G is

$$G = P_2^{-1} R = \begin{bmatrix} M & 2C \\ -C^T & W - C^T M^{-1} C \end{bmatrix}^{-1} \begin{bmatrix} 0 & C \\ 0 & -C^T M^{-1} C \end{bmatrix} \tag{28}$$

The matrix P_2 in (26) can be decomposed into the form:

$$P_2 = \begin{bmatrix} I & 0 \\ -C^T M^{-1} & I \end{bmatrix} \begin{bmatrix} M & 0 \\ 0 & W + C^T M^{-1} C \end{bmatrix} \begin{bmatrix} I & 2M^{-1} C \\ 0 & I \end{bmatrix} \tag{29}$$

From the above decomposition, It is readily apparent that the matrix P_2 is invertible and we have,

$$P_2^{-1} = \begin{bmatrix} I & -2M^{-1} C \\ 0 & I \end{bmatrix} \begin{bmatrix} M & 0 \\ 0 & W + C^T M^{-1} C \end{bmatrix}^{-1} \begin{bmatrix} I & 0 \\ C^T M^{-1} & I \end{bmatrix} \tag{30}$$

Ensuring the convergence of the iterative process (27) is asserted through the subsequent theorem.

Theorem 3 *Assume that M is a positive definite symmetric matrix with dimensions $m \times m$ and let C be a full-rank Toeplitz matrix with dimensions $m \times n$. Then regardless of the initial estimate, the iterative method (27) converges to the unique solution.*

Proof:
Considering the relation expressed in (30), we obtain

$$G = P_2^{-1} R = \begin{bmatrix} I & -2M^{-1} C \\ 0 & I \end{bmatrix} \begin{bmatrix} M & 0 \\ 0 & W + C^T M^{-1} C \end{bmatrix}^{-1} \begin{bmatrix} I & 0 \\ C^T M^{-1} & I \end{bmatrix} \begin{bmatrix} 0 & C \\ 0 & -C^T M^{-1} C \end{bmatrix}$$

$$= \begin{bmatrix} I & -2M^{-1}C \\ 0 & I \end{bmatrix} \begin{bmatrix} M^{-1} & 0 \\ 0 & (W + C^T M^{-1}C)^{-1} \end{bmatrix} \begin{bmatrix} 0 & C \\ 0 & 0 \end{bmatrix}$$

$$= \begin{bmatrix} I & -2M^{-1}C \\ 0 & I \end{bmatrix} \begin{bmatrix} 0 & -M^{-1}C \\ 0 & 0 \end{bmatrix}$$

$$= \begin{bmatrix} 0 & -M^{-1}C \\ 0 & 0 \end{bmatrix}$$

We deduce that all the eigenvalues associated with the matrix G equate to zero. As a result, we establish $\rho(G) < 1$, confirming the theorem's validity.

The incorporation of the preconditioner P_2 necessitates addressing a linear subsystem in the subsequent stages.

$$P_2 z = r = \begin{bmatrix} I & 0 \\ -C^T M^{-1} & I \end{bmatrix} \begin{bmatrix} M & 0 \\ 0 & W + C^T M^{-1}C \end{bmatrix} \begin{bmatrix} I & 2M^{-1}C \\ 0 & I \end{bmatrix} \begin{bmatrix} z_1 \\ z_2 \end{bmatrix} \tag{31}$$

$$P_2 z = r = \begin{bmatrix} r_1 \\ r_2 \end{bmatrix}$$

Subsequently, we can outline a straightforward algorithm for computing $z = P_2^{-1}r$ as follows.

Algorithm 2: Calculation of $z = P_2^{-1}r$

---

1. Solve, $(W - C^T MC)z_1 = r_2 + C^T M^{-1}r_1$ for z_1;

2. Set, $z_2 = -2M^{-1}Cz_1 - M^{-1}r_1$.

In the subsequent discussion, we examine the eigenvalues of the preconditioned matrix $P_2^{-1}A$, offering insights into potential acceleration for Krylov subspace methods.

Theorem 4 *In the realm of matrices, consider two entities: a symmetric positive definite matrix M and a full-rank Toeplitz matrix C, with dimensions $(m \times m)$ and $(m \times n)$ respectively. Then the preconditioner P_2 satisfies,*

$$\sigma(P_2^{-1}A) = 1.$$

Proof:

It is straightforward to confirm that

$$P_2^{-1}A \;=\; I - P_2^{-1}R \;=\; \begin{bmatrix} I & -M^{-1}C \\ 0 & I \end{bmatrix}. \tag{32}$$

This complete theorem.

Effectively implementing the preconditioners $(P1, P2)$ involves a single solve with $W - C^T M^{-1} C$ and two matrix-vector multiplications. The primary computational overhead associated with applying this preconditioner is tied to finding a solution to a system of linear equations using the matrix of coefficient $W - C^T M^{-1} C$. This task can be inherently challenging due to the complete fullness of the matrix, making the formulation of an efficient preconditioner a non-trivial endeavor.

The matrix $W - C^T M^{-1} C$ exhibits symmetry and positive definiteness, allowing for potential exact solutions through sparse Cholesky factorization or approximate solutions using methods like The preconditioned conjugate gradient (PCG) method has garnered attention in recent times. A recent study by Benzi and Faccio [12] has introduced and explored various strategies for effectively solving such linear systems. These systems find applications in various computational domains, including augmented Lagrangian methods addressing PDE-related saddle point problems [13, 31], solving KKT systems in constrained optimization [42], and addressing sparse-dense least squares problems [11, 41]. Their study provides a comprehensive overview of different applications involving such linear systems and introduces various solution methodologies.

5   Numerical Experiments

In this section, we assess the performance of modified versions of the proposed block preconditioner using an illustrative test problem extracted from [22]. The test problem mirrors a 2D flow scenario, featuring substantial variations in permeability within the porous flow domain. Tables 1 provide a comprehensive overview, presenting the cumulative count of outer GMRES iterations and the corresponding CPU time in seconds, labeled as "ITER" and "CPU Time," respectively. The total count of inner GMRES (PCG) iterations necessary for solving the systems described by (14) is documented under "ITER." The iterations conclude upon reaching a specified criterion.

$$\left[\frac{\|Ax_j - b\|_2}{\|b\|_2} \right] \le tol$$

The tables include an assessment of the relative error,calculated concerning the kth approximate solution $x_j = (u_j, p_j)$.

$$\text{Error} := \frac{\|x_j - \hat{x}\|_2}{\|\hat{x}\|_2}$$

The true solution $(\hat{x})$ and its approximation (x_j) represent the exact solution and the solution obtained during the $(k) - th$ iteration. Additionally, we employed random solution vectors as right-hand sides, and the outcomes are averaged over 15 test runs. The iteration counts were rounded to the nearest integer. All computations were performed on a computer featuring an Intel Core i7-10750H CPU @ 2.60 GHz processor and 16.0 GB RAM, utilizing MATLAB.R2020b.
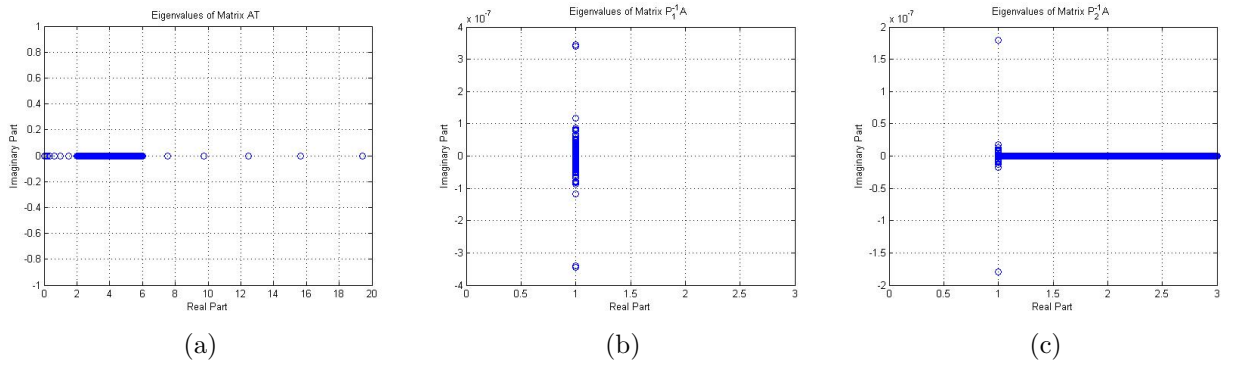

(a)   (b)   (c)

Figure 2: Eigen values distribution of the Darcy problem for the size 2000

Table 1: The results obtained from GMRES and GMRES with (P_1, P_2)

Method	Size	ITER	RELRESI	CPU Time
GMRES	1000	100(10)	0.9374	35.5504
$GMRES\ with\ P_1$	1000	3(3)	1.4615e-4	7.2965
$GMRES\ with\ P_2$	1000	3(4)	0.0014	7.0480
GMRES	1500	140(18)	0.8569	181.5504
$GMRES\ with\ P_1$	1500	3(3)	1.2585e-6	23.0029
$GMRES\ with\ P_2$	1500	3(5)	9.2415e-4	23.6480
GMRES	2000	190(20)	0.9987	427.5504
$GMRES\ with\ P_1$	2000	3(5)	1.1415e-7	43.0480
$GMRES\ with\ P_2$	2000	3(5)	6.5421e-5	43.9657

Remark 1 *Examining Figure 2, it's evident that our new preconditioners (P1, P2) with GMRES exhibit significantly better organization of eigenvalues. In simpler*

15

terms, for our preconditioners, all eigenvalues fall within the range of 1.0 to 3.0 for P2, and they are all at 1.0 for P1. This shows that our suggested method of preparing the data is effective in achieving a more favorable arrangement of eigenvalues.

Remark 2 *The information in Table 1 clearly shows that our newly introduced pre-conditioners GMRES with (P1, P2) consistently achieve the desired level of accuracy very efficiently, regardless of the problem size. It's important to highlight that they rapidly reach the target accuracy, outperforming others in terms of efficiency. The results indicate that the preconditioners GMRES with (P1, P2) methods not only quickly achieve the needed precision but also do so using less CPU time. This strong evidence emphasizes how effective our preconditioner is, demonstrating its ability to use computer resources wisely without compromising accuracy.*

6   Conclusions

In this paper, we introduced a clever way to make solving certain types of mathematical problems faster. This method is specially made for a type of problem related to how fluids move in networks of fractures. We did some math analysis and found a unique pattern in the solutions. When we tested it on a computer using a complex 2D model, our method helped the computer find the solution much faster.

Surprisingly, the GMRES with novel preconditioners (P1, P2) we introduced works a quite better than the simple GMRES method without preconditioner, a common technique for these kinds of problems. GMRES with novel preconditioners (P1, P2) can quickly find the answer with fewer attempts and uses less computer time.

Data availability

Not applicable

Author contribution

These authors contributed equally.

Acknowledgments

Declarations

Human and animal ethics

Not applicable

Competing Interests

The author declares the absence of any competing interests.

References

[1] Clarisse Alboin, Jérôme Jaffré, Jean E Roberts, and Christophe Serres. Modeling fractures as interfaces for flow and transport. *Fluid Flow and Transport in Porous Media, Mathematical and Numerical Treatment*, 295:13, 2002.

[2] Philippe Angot, Franck Boyer, and Florence Hubert. Asymptotic and numerical modelling of flows in fractured porous media. *ESAIM: Mathematical Modelling and Numerical Analysis*, 43(2):239–275, 2009.

[3] Paola F Antonietti, Chiara Facciola, Alessandro Russo, and Marco Verani. Discontinuous galerkin approximation of flows in fractured porous media on polytopic grids. *SIAM Journal on Scientific Computing*, 41(1):A109–A138, 2019.

[4] Douglas N Arnold, Franco Brezzi, Bernardo Cockburn, and L Donatella Marini. Unified analysis of discontinuous galerkin methods for elliptic problems. *SIAM journal on numerical analysis*, 39(5):1749–1779, 2002.

[5] Owe Axelsson. *A survey of robust preconditioning methods*. Springer, 2001.

[6] Owe Axelsson and Vincent Allan Barker. *Finite element solution of boundary value problems: theory and computation*. SIAM, 2001.

[7] Owe Axelsson and Radim Blaheta. Preconditioning of matrices partitioned in 2×2 block form: eigenvalue estimates and schwarz dd for mixed fem. *Numerical Linear Algebra with Applications*, 17(5):787–810, 2010.

[8] Owe Axelsson, Ivo Dravins, and Maya Neytcheva. Stage-parallel preconditioners for implicit runge–kutta methods of arbitrarily high order, linear problems. *Numerical Linear Algebra with Applications*, 31(1):e2532, 2024.

[9] Owe Axelsson and Davod Khojasteh Salkuyeh. A new iteration and preconditioning method for elliptic pde-constrained optimization problems. *Numerical Mathematics: Theory, Methods & Applications*, 13(4), 2020.

[10] Owe Axelsson and Panayot S Vassilevski. Algebraic multilevel preconditioning methods, ii. *SIAM Journal on Numerical Analysis*, 27(6):1569–1590, 1990.

[11] Fariba Bakrani Balani and Masoud Hajarian. A new block preconditioner for weighted toeplitz regularized least-squares problems. *International Journal of Computer Mathematics*, 100(12):2241–2250, 2023.

[12] Michele Benzi and Chiara Faccio. Solving linear systems of the form by preconditioned iterative methods. *SIAM Journal on Scientific Computing*, pages S51–S70, 2023.

[13] Michele Benzi and Maxim A Olshanskii. An augmented lagrangian-based approach to the oseen problem. *SIAM Journal on Scientific Computing*, 28(6):2095–2113, 2006.

[14] Stefano Berrone, Sandra Pieraccini, and Stefano Scialo. On simulations of discrete fracture network flows with an optimization-based extended finite element method. *SIAM Journal on Scientific Computing*, 35(2):A908–A935, 2013.

[15] Wietse M Boon, Jan M Nordbotten, and Ivan Yotov. Robust discretization of flow in fractured porous media. *SIAM Journal on Numerical Analysis*, 56(4):2203–2233, 2018.

[16] Erik Burman, Susanne Claus, Peter Hansbo, Mats G Larson, and André Massing. Cutfem: discretizing geometry and partial differential equations. *International Journal for Numerical Methods in Engineering*, 104(7):472–501, 2015.

[17] Raymond H Chan, Xiao-Qing Jin, and Yue-Hung Tam. Strang-type preconditioners for solving systems of odes by boundary value methods. *Electronic Journal of Mathematical and Physical Sciences*, 1(1):14–46, 2002.

[18] Raymond H Chan and Michael K Ng. Iterative methods for linear systems with matrix structure. In *Fast reliable algorithms for matrices with structure*, pages 117–152. SIAM, 1999.

[19] Raymond H Chan, Michael K Ng, and Xiao-Qing Jin. Strang-type preconditioners for systems of lmf-based ode codes. *IMA journal of numerical analysis*, 21(2):451–462, 2001.

[20] Raymond H Chan, Daniel Potts, and Gabriele Steidl. Preconditioners for non-hermitian toeplitz systems. *Numerical linear algebra with applications*, 8(2):83–98, 2001.

[21] Florent Chave, Daniele Di Pietro, and Luca Formaggia. High-order method for darcy flows in fractured porous media. *arXiv preprint arXiv:1711.11420*, 2017.

[22] Alexey Y Chernyshenko and Maxim A Olshanskii. An unfitted finite element method for the darcy problem in a fracture network. *Journal of Computational and Applied Mathematics*, 366:112424, 2020.

[23] Alexey Y Chernyshenko, Maxim A Olshanskii, and Yuri V Vassilevski. A hybrid finite volume–finite element method for bulk–surface coupled problems. *Journal of Computational Physics*, 352:516–533, 2018.

[24] Klaus Deckelnick, Charles M Elliott, and Thomas Ranner. Unfitted finite element methods using bulk meshes for surface partial differential equations. *SIAM Journal on Numerical Analysis*, 52(4):2137–2162, 2014.

[25] Michael J Economides, Kenneth G Nolte, et al. *Reservoir stimulation*, volume 2. Prentice Hall Englewood Cliffs, NJ, 1989.

[26] Bernd Flemisch, Inga Berre, Wietse Boon, Alessio Fumagalli, Nicolas Schwenck, Anna Scotti, Ivar Stefansson, and Alexandru Tatomir. Benchmarks for single-phase flow in fractured porous media. *Advances in Water Resources*, 111:239–258, 2018.

[27] Bernd Flemisch, Alessio Fumagalli, and Anna Scotti. A review of the xfem-based approximation of flow in fractured porous media. *Advances in Discretization Methods: Discontinuities, Virtual Elements, Fictitious Domain Methods*, pages 47–76, 2016.

[28] Luca Formaggia, Alessio Fumagalli, Anna Scotti, and Paolo Ruffo. A reduced model for darcy's problem in networks of fractures. *ESAIM: Mathematical Modelling and Numerical Analysis*, 48(4):1089–1116, 2014.

[29] Najla Frih, Vincent Martin, Jean Elizabeth Roberts, and Ali Saâda. Modeling fractures as interfaces with nonmatching grids. *Computational Geosciences*, 16:1043–1060, 2012.

[30] Alessio Fumagalli, Eirik Keilegavlen, and Stefano Scialò. Conforming, non-conforming and non-matching discretization couplings in discrete fracture network simulations. *Journal of Computational Physics*, 376:694–712, 2019.

[31] Gene H Golub and Chen Greif. On solving block-structured indefinite linear systems. *SIAM Journal on Scientific Computing*, 24(6):2076–2092, 2003.

[32] Anita Hansbo and Peter Hansbo. An unfitted finite element method, based on nitsche's method, for elliptic interface problems. *Computer methods in applied mechanics and engineering*, 191(47-48):5537–5552, 2002.

[33] Peter Hansbo, Mats G Larson, and André Massing. A stabilized cut finite element method for the darcy problem on surfaces. *Computer Methods in Applied Mechanics and Engineering*, 326:298–318, 2017.

[34] Hao Huang, Ted A Long, Jing Wan, and William P Brown. On the use of enriched finite element method to model subsurface features in porous media flow problems. *Computational Geosciences*, 15:721–736, 2011.

[35] Markus Köppel, Vincent Martin, and Jean E Roberts. A stabilized lagrange multiplier finite-element method for flow in porous media with fractures. *GEM-International Journal on Geomathematics*, 10(1):7, 2019.

[36] Vincent Martin, Jérôme Jaffré, and Jean E Roberts. Modeling fractures and barriers as interfaces for flow in porous media. *SIAM Journal on Scientific Computing*, 26(5):1667–1691, 2005.

[37] Arif Masud and Thomas JR Hughes. A stabilized mixed finite element method for darcy flow. *Computer methods in applied mechanics and engineering*, 191(39-40):4341–4370, 2002.

[38] Maxim A Olshanskii and Arnold Reusken. Trace finite element methods for pdes on surfaces. In *Geometrically Unfitted Finite Element Methods and Applications: Proceedings of the UCL Workshop 2016*, pages 211–258. Springer, 2017.

[39] Maxim A Olshanskii, Arnold Reusken, and Jörg Grande. A finite element method for elliptic equations on surfaces. *SIAM journal on numerical analysis*, 47(5):3339–3358, 2009.

[40] Arnold Reusken. Analysis of trace finite element methods for surface partial differential equations. *IMA Journal of Numerical Analysis*, 35(4):1568–1590, 2015.

[41] Jennifer A Scott and Miroslav Tuma. Sparse stretching for solving sparse-dense linear least-squares problems. *SIAM Journal on Scientific Computing*, 41(3):A1604–A1625, 2019.

[42] Stephen J Wright. *Numerical optimization.* 2006.

[43] Mark D Zoback. *Reservoir geomechanics.* Cambridge university press, 2010.